Global resurfacing of Uranus's moon Miranda by convection

Noah P. Hammond* and Amy C. Barr*
Department of Geological Sciences, Brown University, 324 Brook Street, Providence, Rhode Island 02912, USA

ABSTRACT

Miranda, an icy moon of Uranus, is one of the most visually striking and enigmatic bodies in the solar system. Three polygonal-shaped regions of intense deformation, dubbed "coronae," dominate the surface of Miranda. Here we use numerical methods to show that sluggish-lid convection in Miranda's ice shell, powered by tidal heating, can simultaneously match the global distribution of coronae, the concentric deformation pattern, and the estimated heat flow during formation. The expected rheological conditions in Miranda's ice shell lead to the development of low-order convection that produces surface deformation patterns similar to those observed. We find that satellite core size strongly controls convection geometry and that low-order convection patterns are much more stable for core radii less than half the satellite radius.

INTRODUCTION

Miranda, the innermost regular satellite of Uranus, has an average radius, *R,* of 235.8 km (Thomas, 1988), and a mean density of 1.2 g cm^{-3} (Jacobson et al., 1992), suggesting a mixed ice and rock composition. Miranda orbits Uranus at a distance of 5.11 Uranus radii, and its current eccentricity, *e,* is 0.0013. Despite its relatively small size, Miranda appears to have experienced an episode of intense endogenic resurfacing (Smith et al., 1986), resulting in the formation of at least three remarkable and unique surface features called "coronae." Each corona is at least 200 km across, is ovoidal or polygonal in shape (see Fig. 1), and is surrounded by an outer belt of concentric, sub-parallel ridges and troughs (Smith et al., 1986). Arden corona, the largest, has ridges and troughs with up to 2 km of relief, whose slopes and orientations are consistent with tilt-block–style normal faults (Pappalardo et al., 1997). Elsinore corona has an outer belt that is ~80 km wide, relatively smooth, and elevated above the surrounding terrain by ~100 m (Schenk, 1991). Inverness corona has a trapezoidal shape with a large bright chevron at its center. The northern hemisphere of Miranda was never imaged by the *Voyager 2* spacecraft, so it is unknown whether additional coronae exist.

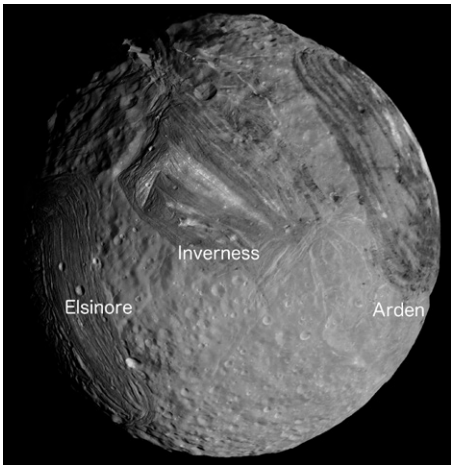

Figure 1. Mosaic of southern hemisphere of Miranda, the innermost regular satellite of Uranus, with radius of 236 km. Projection is orthographic, centered on the south pole. Visible from left to right are Elsinore, Inverness, and Arden coronae. Images credit: NASA/Jet Propulsion Laboratory/Ted Stryk.

*E-mails: noah_hammond@brown.edu; amy_c_mlinar@brown.edu.

Many hypotheses have been put forth to propose how the coronae formed. One hypothesis is that Miranda was catastrophically disrupted and reassembled, and that coronae formed as a result of silicate material sinking through an icy mantle, causing concentric surface contraction (Janes and Melosh, 1988). In contrast, the majority of researchers suggest that coronae likely formed as the result of buoyant diapirs causing surface extension (Croft and Soderblom, 1991; Greenberg et al., 1991; Pappalardo et al., 1997). Geologic interpretations suggesting that the coronae are composed of extensional tectonic and volcanic landforms support the hypothesis that coronae formed in an extensional environment (Schenk, 1991; Pappalardo et al., 1997). It has also been suggested that heat generated during tidal flexing played an important role in corona formation (Dermott et al., 1988; Pappalardo et al., 1997), but the way in which internal heating leads to the observed surface deformation has not been well described.

Here we simulate convection in Miranda's ice shell to test the hypothesis that coronae formed by convection-driven resurfacing during an episode of tidal heating. We show that if the surface is weak, sluggish-lid convection can occur, which simultaneously produces the estimated heat flow, the deformation pattern within the coronae, and the approximate number of upwellings needed to form the coronae.

FORMATION CONDITIONS

Models of lithospheric flexure along the flanks of Arden corona suggest an elastic thickness of 2 km and a thermal gradient of 8–20 K km^{-1} during corona formation (Pappalardo et al., 1997). For a thermal conductivity, *k*, of 5 W m^{-1} K^{-1} (Petrenko and Whitworth, 1999), this corresponds to a heat flux of 40–100 mW m^{-2}. Such a high heat flow implies the past existence of thermal anomalies beneath the coronae, powered by a heat source other than radiogenic heating, which is not expected to be significant (Greenberg et al., 1991). One likely heat source is tidal dissipation in the ice shell, which can occur when the time-varying tidal potential during an eccentric orbit causes a satellite to be repeatedly stretched and squeezed (e.g., Ojakangas and Stevenson, 1989). Several studies suggest that a past 3:1 orbital resonance between Miranda and neighboring satellite Umbriel can explain Miranda's present orbital inclination of 4.5° (Dermott et al., 1988; Tittemore and Wisdom, 1989; Malhotra and Dermott, 1990; Verheylewegen et al., 2013). During this resonance, Miranda's eccentricity may have been excited to $e = 0.05$ (Malhotra and Dermott, 1990). If Miranda were as dissipative as Saturn's satellite Enceladus, which is similar in size, composition, and orbital frequency to Miranda, we calculate that tidal dissipation could have generated as much as 5 GW of power (cf. Peale and Cassen, 1978), for a Miranda with a quality factor $Q = 20$ and Love number $k_2 = 9.3 \times 10^{-4}$ (Item DR1 in the GSA Data Repository[1]). Tidal dissipation focused in relatively warm ice at depth could have created conditions more favorable for convection by raising the thermal gradient across the ice shell and lowering the viscosity of ice.

For convection to drive surface deformation, on either terrestrial planets or icy satellites, the surface must behave much more weakly than predicted by laboratory experiments (Tackley, 1993; Showman and Han, 2005). Convection with strongly temperature-dependent viscosity predicts that vigorous fluid motion would be confined below a thick, undeforming stagnant lid (Solomatov 1995). For convection to reach the surface, convective stresses must overcome the yield strength in the lid (e.g., Moresi and Solomatov, 1998). Once the yield strength is overcome, the surface deforms with strain rates similar to those of systems in the sluggish-lid regime (Solomatov, 1995), which have moder-

[1]GSA Data Repository item 2014335, detailed description of our tidal heating calculations (Item DR1), a discussion of convective stresses (Item DR2), and benchmarking for our convection calculations (Item DR3), is available online at www.geosociety.org/pubs/ft2014.htm, or on request from editing@geosociety.org or Documents Secretary, GSA, P.O. Box 9140, Boulder, CO 80301, USA.

ately low-viscosity contrasts between the top and bottom of the mantle.

Following scaling laws of Solomatov (2004), we calculate that convective stresses could have deformed the surface of Miranda if its effective surface yield stress is ~10 kPa (Item DR2). Similar yield-stress values have been inferred for Enceladus, where near-surface convection is thought to generate the observed thermal anomaly in the geologically active South Polar Terrain (Barr, 2008; O'Neill and Nimmo, 2010). Additionally, the surfaces of Europa and Enceladus fail in response to daily tidal stresses of ~20 kPa (Hoppa et al., 1999; Hurford et al., 2007). Laboratory and field experiments, however, suggest that the yield stress of ice is an order of magnitude higher, ~0.1–1 MPa (Kehle 1964), implying that the lithospheres of tidally flexed satellites may be anomalously weak.

MODELING CONVECTION-DRIVEN CORONA FORMATION

We simulate convection in Miranda's ice mantle for a wide range of initial conditions using the three-dimensional (3-D) spherical convection model CitcomS (Zhong et al., 2000; Tan et al., 2006). We explore three different sizes for Miranda's rock core: (1) core radius to satellite radius fraction $x = 0.55$, corresponding to a core composed of low-density rock (2.5 g cm^{-3}), (2) $x = 0.4$, appropriate for rock density 3.5 g cm^{-3}, and (3) $x = 0.25$, appropriate for a partially differentiated body with an ice mantle containing 10% rock by volume.

We vary the Rayleigh number, which governs the vigor of convection, as

$$Ra = \frac{\rho_i g \alpha \Delta T D^3}{\kappa \eta_b}, \quad (1)$$

where the density of ice $\rho_i = 920$ kg m^{-3}, the acceleration due to gravity $g = 0.083$ m s^{-2}, the thermal expansivity $\alpha = 1.56 \times 10^{-4}$ $(T_i / 250\ \mathrm{K})$ K^{-1} (T_i is the average internal temperature) (Kirk and Stevenson, 1987), the temperature contrast across the ice shell is $\Delta T = T_b - T_s$ (b is base, s is surface), the ice shell thickness $D = (1 - x) \times R_{satellite}$, the thermal diffusivity $\kappa = 1.47 \times 10^{-6}$ $(250\ \mathrm{K} / T_i)^2$ m^2 s^{-1} (Kirk and Stevenson, 1987), and η_b is the viscosity of ice at the base. The surface temperature, T_s, is 60 K and the temperature at the base of the ice shell, T_b, is 220–270 *K*. Over this range of T_b, for a grain size $d = 0.2$ mm, the viscosity of ice deforming by volume diffusion is $\eta_b = 10^{14}$–10^{17} Pa s (Goldsby and Kohlstedt, 2001; Barr and Pappalardo, 2005; Barr and McKinnon, 2007), yielding $Ra = 10^4$–10^8 (Item DR3).

Throughout the ice shell, viscosity varies as

$$\eta(T) = \eta_b \exp(-\gamma T), \quad (2)$$

where $\gamma = \theta / \Delta T$, $\theta = \ln(\Delta\eta)$, and $\Delta\eta$ is the effective viscosity contrast across the ice shell. We assume sluggish-lid convection, limiting $\Delta\eta$ to 10^3–10^4 to mimic the effect of surface ice with a low yield stress (e.g., King et al., 1992; Trompert and Hansen, 1998; Moresi and Solomatov, 1998). The surface Rayleigh number $Ra_s = Ra/\Delta\eta$. The majority of our simulations are started with an initially conductive temperature profile with a small temperature perturbation near the base and free-slip boundary conditions at the top and bottom of the ice shell. We run simulations until the surface heat flow approaches steady state, and record the velocity and thermal gradient at the surface.

We are interested in whether convection in Miranda's ice shell leads to surface deformation patterns that resemble the distribution of the coronae, but the number of convective plumes and their arrangement has been shown to be affected by core size (Deschamps et al., 2010), viscosity structure, Rayleigh number (Schubert et al., 2001), and the distribution of tidal heating (Han and Showman, 2010). It is difficult to determine which of these variables has the largest influence on convection geometry.

In order to independently address each of these effects, we use three different approaches. First we use a simplified approach where we apply an initial temperature perturbation (of spherical harmonic order $l = 3$, $m = 2$) that pushes the system toward low-order tetrahedral convection (e.g., Ratcliff et al., 1996). We then vary Ra, $\Delta\eta$, and x to determine the parameter space over which low-order convection can remain stable. In this suite of simulations, the temperature at the base of the ice shell is held constant, representing tidal energy focused on warm low-viscosity ice at depth. Our second approach is designed to assess the influence of the initial temperature condition. We re-run simulations that led to low-order convection in the first suite of simulations using a random initial temperature perturbation.

Finally, we explore how the distribution of tidal heating might affect convection geometry. For a satellite with a subsurface ocean, a degree-2 pattern is expected to dominate, where heating concentrates near the poles (Tobie et al., 2005). Without an ocean, tidal strain near the base of the ice shell may concentrate near the equator in a cubic-type pattern (see Tobie et al., 2005; Beuthe, 2013). By assuming that tidal heating heterogeneously warmed the ice shell to generate the initial temperature condition, we represent these patterns as the sum of spherical harmonic temperature perturbations, following the equations given by Beuthe (2013).

RESULTS

We find that rheological conditions in Miranda's ice shell favor the development of low-order convection patterns. Core size strongly controls convection geometry. Models of Miranda with a core radius fraction $x = 0.55$ generally develop higher-order convective patterns, whereas Miranda with a core radius fraction $x = 0.25$ can sustain tetrahedral convection over the broadest range of rheological constraints (Fig. 2A), probably because longer-wavelength plumes are preferred as core radius fraction decreases (Schubert et al., 2001; Deschamps et al., 2010). For simulations with low-order convection and with surface Rayleigh numbers between 10^2 and $10^{3.5}$, the average thermal gradient in regions of surface extension is remarkably consistent with estimates suggested from lithospheric flexure (Fig. 2B). This shows that sluggish-lid convection can simultaneously match the estimated thermal gradient and the approximate number of upwellings necessary to form the coronae. We consider the successful range in plume number to be 4–6, because there are three coronae visible in the southern hemisphere of Miranda. Simulations with random initial temperature perturbations and a fractional core radius of $x = 0.25$ also develop low-order convection patterns (Fig. 3). This shows that low-order convection

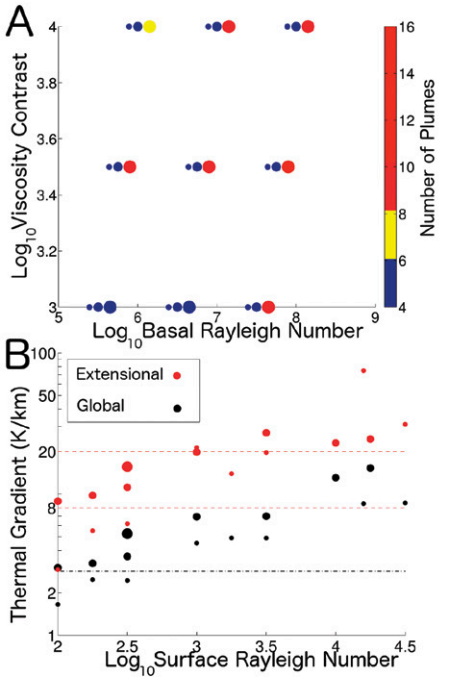

Figure 2. A: Convection models from our first set of simulations as a function of basal Rayleigh number and viscosity contrast. Symbol color indicates number of plumes present after convection approaches steady state. Symbol size scales with fractional size of the rocky core, *x* = 0.25, 0.4, and 0.55. B: Surface Rayleigh number versus thermal gradient for simulations with stable low-order convection. Red points show thermal gradient in regions of extension; black points show global average. Red dashed lines indicate extensional thermal gradient implied by models of lithospheric flexure (Pappalardo et al., 1997). Black dashed line indicates that total surface power of 10 GW is necessary to provide global thermal gradient of ~3 K km^{-1}, given a thermal conductivity of 5 W m^{-1} K^{-1}.

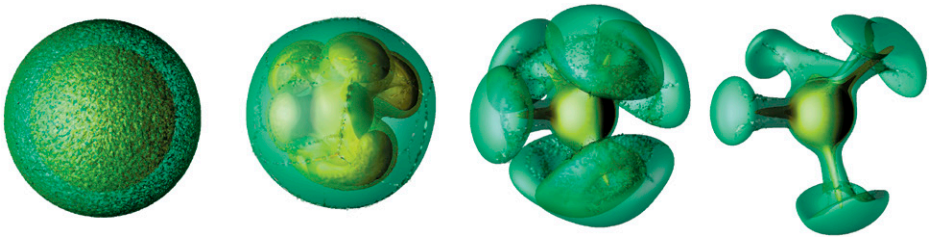

Figure 3. Time evolution of convection in Uranus' moon Miranda's ice shell started with random initial temperature perturbations throughout the base of the ice shell, with Rayleigh number $Ra = 10^{6.5}$, $\Delta\eta = 10^3$ (effective viscosity contrast across the ice shell), fractional core size $x = 0.25$, and basal heating. Colors represent temperature isosurfaces, with green and yellow corresponding to 120 K and 170 K, respectively. The convective upwellings merge until reaching a low-order convection pattern with ~5 plumes.

easily develops in systems with low Rayleigh numbers, low effective-viscosity contrasts, and small core sizes, regardless of the initial temperature condition. Simulations run with a zero-slip condition at the base of the ice shell had slightly lower Nusselt numbers than those with a free-slip condition, but the convection geometry was unaffected.

We also find that convection in Miranda's ice shell produces the concentric deformation pattern within the coronae. Figure 4 shows the surface velocity field and near-surface thermal gradient resulting from two different convection simulations. Above convective upwellings, the thermal gradient is elevated to values predicted from flexure, and the surface extends concentrically away from the center, similar to the predicted formation environment of the coronae (Greenberg et al., 1991). Surface deformation patterns resulting from tetrahedral convection (e.g., Ratcliff et al., 1996), shown in Figure 4B, can match the locations of two of the coronae, but a third upwelling occurs where no surface deformation is observed.

To match the exact locations of all of the coronae, we must invoke a tidal heating pattern predicted for an icy satellite with no ocean (Tobie et al., 2005; Beuthe, 2013). In this case, four plumes are generated near the equator, each separated by ~90°. Inverness corona is located near the south pole, so in order for this convection pattern to be consistent with the current locations of the coronae, a reorientation is required. Figure 4C shows surface deformation patterns produced by this style of convection after a 60° rotation from the sub-Uranian point at the equator toward the south pole. Convective upwellings occur almost precisely beneath the locations of Arden, Inverness, and Elsinore coronae, and the size of extensional regions above the upwellings are in good agreement with the sizes of the coronae. Similar reorientations of Miranda have been suggested on the basis of the skewed impact-crater distribution (Plescia, 1988) and the orientation of scarps that might have been influenced by stresses from reorientation (Pappalardo, 1994). The reorientation of a convective upwelling toward the poles is also suggested to have occurred on Enceladus (e.g., Nimmo and Pappalardo, 2006).

DISCUSSION

We find that convection in Miranda's ice shell powered by tidal heating can generate the global distribution of coronae, the concentric orientation of sub-parallel ridges and troughs, and the thermal gradient implied by flexure. Models that account for the possible distribution of tidal heating can even match the precise locations of the coronae, after a reorientation of 60°. Two aspects of corona morphology that do not arise naturally in our model are the angular shapes of the coronae and their differences in morphology. Pappalardo (1994) suggested that the angular appearance may have resulted from radial stresses that interacted with preexisting fractures. We suggest that differences in corona morphology might be partly explained by variations in extensional strain rates, because spreading rate can control the tectonic expression of mid-ocean ridges on Earth (Phipps Morgan and Chen, 1993).

Simulations that match the thermal gradient from flexure have total power outputs of close to 10 GW (Fig. 2B), somewhat larger than the total power we predict could be generated during orbital resonance. One explanation for this discrepancy is that the thermal gradient inferred at Arden corona may not apply to Inverness or Elsinore coronae, so convection need not produce the inferred thermal gradient at each upwelling at the same time. Alternatively, it is possible that convection may have episodically deformed the surface, leading to temporary, dramatic increases in surface heat flux (e.g., Moresi and Solomatov, 1998; O'Neill and Nimmo, 2010). In any case, Miranda must be at least as dissipative as Enceladus for tidal heating to power convection, and may be required to have entered orbital resonance already warm and dissipative, because tidal heating models predict that it is difficult to warm up Miranda from an initially cool state (E. Verheylewegen, 2014, personal commun.). Further studies that incorporate a finite yield stress, and incorporate more complex treatments of tidal heating into spherical convection models, could explore the possible time-dependent behavior of corona formation and the feedback between tidal heating and thermal plumes.

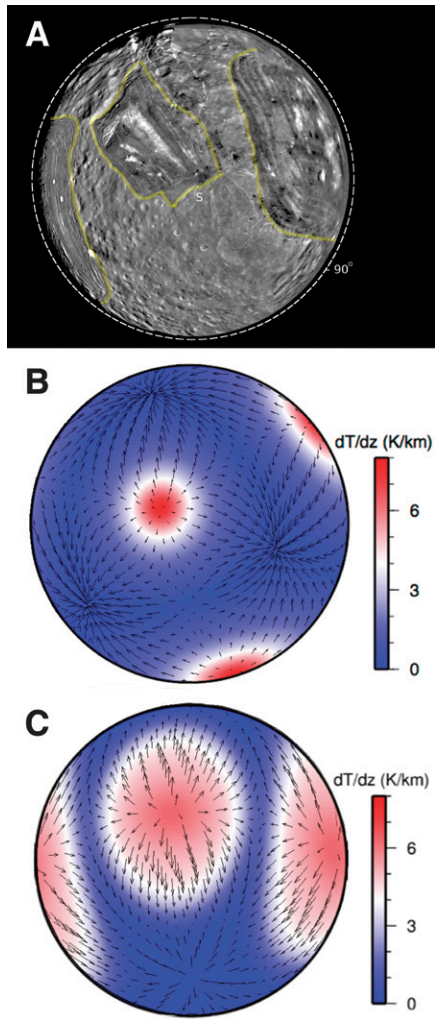

Figure 4. A: Mosaic of Uranus' moon Miranda's southern hemisphere with coronae outlined in yellow. Projection is orthographic centered on the south pole. Dashed white line approximates the equator. B, C: Surface conditions of convection simulations, plotted within same projection as A, with near-surface thermal gradient indicated by color, and arrows denoting surface velocity. Above convective upwellings, the thermal gradient is consistent with values predicted from flexure, and the surface is undergoing concentric surface extension. Steady-state tetrahedral convection is shown in B, with Rayleigh number $Ra = 10^{6.75}$, $\Delta\eta = 10^{3.5}$ (effective viscosity contrast across the ice shell), and fractional core size $x = 0.4$. Convection in C results from concentrated tidal heating near the equator, predicted for a satellite with no ocean (Beuthe, 2013), after a 60° rotation from the sub-Uranian point toward the south pole. .

ACKNOWLEDGMENTS

This work is supported by NASA Earth and Space Science Fellowship NNX13AN99H and NASA Planetary Geology and Geophysics Program NNX12AI76G. We thank S. King, J. Roberts, and an anonymous reviewer for helpful comments.

REFERENCES CITED

Barr, A.C., 2008, Mobile lid convection beneath Enceladus' south polar terrain: Journal of Geophysical Research, v. 113, E07009, doi:10.1029/2008JE003114.

Barr, A.C., and McKinnon, W.B., 2007, Convection in Enceladus' ice shell: Conditions for initiation: Geophysical Research Letters, v. 34, L09202, doi:10.1029/2006GL028799.

Barr, A.C., and Pappalardo, R.T., 2005, Onset of convection in the icy Galilean satellites: Influence of rheology: Journal of Geophysical Research, v. 110, E12005, doi:10.1029/2004JE002371.

Beuthe, M., 2013, Spatial patterns of tidal heating: Icarus, v. 223, p. 308–329, doi:10.1016/j.icarus.2012.11.020.

Croft, S.K., and Soderblom, L.A., 1991, Geology of the Uranian satellites, *in* Bergstralh, J.T., Miner, E.D., and Matthews, M.S., eds., Uranus: Tucson, University of Arizona Press, p. 561–628.

Dermott, S.F., Malhotra, R., and Murray, C.D., 1988, Dynamics of the Uranian and Saturnian satellite systems: A chaotic route to melting Miranda?: Icarus, v. 76, p. 295–334, doi:10.1016/0019-1035(88)90074-7.

Deschamps, F., Tackley, P.J., and Nakagawa, T., 2010, Temperature and heat flux scalings for isoviscous thermal convection in spherical geometry: Geophysical Journal International, v. 182, p. 137–154.

Goldsby, D.L., and Kohlstedt, D.L., 2001, Superplastic deformation of ice: Experimental observations: Journal of Geophysical Research, v. 106, p. 11,017–11,030, doi:10.1029/2000JB900336.

Greenberg, R., Croft, S.K., Janes, D.M., Kargel, J.S., Lebofsky, L.A., Lunine, J.I., Marcialis, R.L., Melosh, H.J., Ojakangas, G.W., and Strom, R.G., 1991, Miranda, *in* Bergstralh, J.T., Miner, E.D., and Matthews, M.S., eds., Uranus: Tucson, University of Arizona Press, p. 693–735.

Han, L., and Showman, A.P., 2010, Coupled convection and tidal dissipation in Europa's ice shell: Icarus, v. 207, p. 834–844, doi:10.1016/j.icarus.2009.12.028.

Hoppa, G.V., Tufts, B.R., Greenberg, R., and Geissler, P.E., 1999, Formation of cycloidal features on Europa: Science, v. 285, p. 1899–1902, doi:10.1126/science.285.5435.1899.

Hurford, T.A., Helfenstein, P., Hoppa, G.V., Greenberg, R., and Bills, B.G., 2007, Eruptions arising from tidally controlled periodic openings of rifts on Enceladus: Nature, v. 447, p. 292–294, doi:10.1038/nature05821.

Jacobson, R.A., Campbell, J.K., Taylor, A.H., and Synnott, S.P., 1992, The masses of Uranus and its major satellites from Voyager tracking data and Earth-based Uranian satellite data: The Astronomical Journal, v. 103, p. 2068–2078, doi:10.1086/116211.

Janes, D.M., and Melosh, H.J., 1988, Sinker tectonics: An approach to the surface of Miranda: Journal of Geophysical Research, v. 93, p. 3127–3143, doi:10.1029/JB093iB04p03127.

Kehle, R.O., 1964, Deformation of the Ross ice shelf, Antarctica: Geological Society of America Bulletin, v. 75, p. 259–286, doi:10.1130/0016-7606(1964)75[259:DOTRIS]2.0.CO;2.

King, S.D., Gable, C.W., and Weinstein, S.A., 1992, Models of convection-driven tectonic plates: A comparison of methods and results: Geophysical Journal International, v. 109, p. 481–487, doi:10.1111/j.1365-246X.1992.tb00111.x.

Kirk, R.L., and Stevenson, D.J., 1987, Thermal evolution of a differentiated Ganymede and implications for surface features: Icarus, v. 69, p. 91–134, doi:10.1016/0019-1035(87)90009-1.

Malhotra, R., and Dermott, S.F., 1990, The role of secondary resonances in the orbital history of Miranda: Icarus, v. 85, p. 444–480, doi:10.1016/0019-1035(90)90126-T.

Moresi, L., and Solomatov, V., 1998, Mantle convection with a brittle lithosphere: Thoughts on the global tectonic styles of the Earth and Venus: Geophysical Journal International, v. 133, p. 669–682, doi:10.1046/j.1365-246X.1998.00521.x.

Nimmo, F., and Pappalardo, R.T., 2006, Diapir-induced reorientation of Saturn's moon Enceladus: Nature, v. 441, p. 614–616, doi:10.1038/nature04821.

Ojakangas, G.W., and Stevenson, D.J., 1989, Thermal state of an ice shell on Europa: Icarus, v. 81, p. 220–241, doi:10.1016/0019-1035(89)90052-3.

O'Neill, C., and Nimmo, F., 2010, The role of episodic overturn in generating the surface geology and heat flow on Enceladus: Nature Geoscience, v. 3, p. 88–91, doi:10.1038/ngeo731.

Pappalardo, R.T., 1994, The origin and evolution of ridge and trough terrain and the geological history of Miranda [Ph.D. thesis]: Tempe, Arizona State University, 470 p.

Pappalardo, R.T., Reynolds, S.J., and Greeley, R., 1997, Extensional tilt blocks on Miranda: Evidence for an upwelling origin of Arden Corona: Journal of Geophysical Research, v. 102, p. 13,369–13,379, doi:10.1029/97JE00802.

Peale, S., and Cassen, P., 1978, Contribution of tidal dissipation to lunar thermal history: Icarus, v. 36, p. 245–269, doi:10.1016/0019-1035(78)90109-4.

Petrenko, V.F., and Whitworth, R.W., 1999, Physics of Ice: Oxford, New York, Oxford University Press, 373 p.

Phipps Morgan, J., and Chen, Y.J., 1993, Dependence of ridge-axis morphology on magma supply and spreading rate: Nature, v. 364, p. 706–708, doi:10.1038/364706a0.

Plescia, J.B., 1988, Cratering history of Miranda: Implications for geologic processes: Icarus, v. 73, p. 442–461, doi:10.1016/0019-1035(88)90055-3.

Ratcliff, J.T., Schubert, G., and Zebib, A., 1996, Effects of temperature-dependent viscosity on thermal convection in a spherical shell: Physica D: Nonlinear Phenomena, v. 97, p. 242–252, doi:10.1016/0167-2789(96)00150-9.

Schenk, P.M., 1991, Fluid volcanism on Miranda and Ariel: Flow morphology and composition: Journal of Geophysical Research, v. 96, p. 1887–1906, doi:10.1029/90JB01604.

Schubert, G., Turcotte, D.L., and Olson, P., 2001, Mantle Convection in the Earth and Planets: Cambridge, UK, Cambridge University Press, 940 p.

Showman, A.P., and Han, L., 2005, Effects of plasticity on convection in an ice shell: Implications for Europa: Icarus, v. 177, p. 425–437, doi:10.1016/j.icarus.2005.02.020.

Smith, B.A., et al., 1986, Voyager 2 in the Uranian system: Imaging science results: Science, v. 233, p. 43–64, doi:10.1126/science.233.4759.43.

Solomatov, V.S., 1995, Scaling of temperature- and stress-dependent viscosity convection: Physics of Fluids, v. 7, p. 266–274, doi:10.1063/1.868624.

Solomatov, V.S., 2004, Initiation of subduction by small-scale convection: Journal of Geophysical Research, v. 109, B01412, doi:10.1029/2003JB002628.

Tackley, P.J., 1993, Effects of strongly temperature-dependent viscosity on time-dependent, three-dimensional models of mantle convection: Geophysical Research Letters, v. 20, p. 2187–2190, doi:10.1029/93GL02317.

Tan, E., Choi, E., Thoutireddy, P., Gurnis, M., and Aivazis, M., 2006, GeoFramework: Coupling multiple models of mantle convection within a computational framework: Geochemistry Geophysics Geosystems, v. 7, Q06001, doi:10.1029/2005GC001155.

Thomas, P.C., 1988, Radii, shapes, and topography of the satellites of Uranus from limb coordinates: Icarus, v. 73, p. 427–441, doi:10.1016/0019-1035(88)90054-1.

Tittemore, W.C., and Wisdom, J., 1989, Tidal evolution of the Uranian satellites: II. An explanation of the anomalously high orbital inclination of Miranda: Icarus, v. 78, p. 63–89, doi:10.1016/0019-1035(89)90070-5.

Tobie, G., Grasset, O., Lunine, J.I., Mocquet, A., and Sotin, C., 2005, Titan's internal structure inferred from a coupled thermal-orbital model: Icarus, v. 175, p. 496–502, doi:10.1016/j.icarus.2004.12.007.

Trompert, R., and Hansen, U., 1998, Mantle convection simulations with rheologies that generate plate-like behavior: Nature, v. 395, p. 686–689, doi:10.1038/27185.

Verheylewegen, E., Noyelles, B., and Lemaitre, A., 2013, A numerical exploration of Miranda's dynamical history: Monthly Notices of the Royal Astronomical Society, v. 435, p. 1776–1787, doi:10.1093/mnras/stt1415.

Zhong, S., Zuber, M.T., Moresi, L., and Gurnis, M., 2000, Role of temperature-dependent viscosity and surface plates in spherical shell models of mantle convection: Journal of Geophysical Research, v. 105, p. 11,063–11,082, doi:10.1029/2000JB900003.

Manuscript received 25 July 2014
Revised manuscript received 4 August 2014
Manuscript accepted 4 August 2014

Printed in USA